Progress In Electromagnetics Research B, Vol. 70, 27–40, 2016

Detection of Metal Objects near a Random Rough Surface of Medium at Sounding by Orthogonally Polarized Ultrawideband Pulses

Vladimir I. Koshelev*, Andrey A. Petkun, and Vyacheslav M. Tarnovsky

Abstract—Using the program of numerical simulation of ultrawideband pulse reflection from dielectric medium with random rough surface, a possibility to detect ideally conducting objects placed near the surface was investigated. Medium parameters corresponded to the cases of the dry and wet sandy ground. Based on the correlation analysis of the reflected objects with orthogonal polarizations, a decision about the presence or absence of an object was made. An ideally conducting rectangular object was buried into the ground with a random rough surface to different depth. A cross-shaped metal object was disposed above the surface.

1. INTRODUCTION

One of the branches of electrodynamic researches is development of methods for detection and recognition of objects, including biological ones, in the conditions complicating direct object observation by means of optical devices. Among the problems under solution, one can mark object detection against the background of a random rough surface (RRS). It can be both a ground surface with vegetation and a waved sea surface.

A traditional device for the ground object recognition is ground penetrating radar (GPR) [1]. Usually, it presents bistatic land-based radar. So, in order to use GPR, it is necessary to have direct access to the search area. For remote object detection, a synthetic aperture method is often used [2, 3]. However, for the radar imaging of the search area, certain time is also necessary for steering. Development of the methods for the object detection near RRS in the real-time mode, e.g., by means of aerial devices, is of importance. Herewith, a sounding signal should be ultrawideband to increase the information capability, and received reflected signals should be exposed to the fast correlation processing [4].

A number of papers consider new methods of object detection against the background of a RRS. In [5, 6], not only fields scattered by a random surface but also responses of common targets are considered. It is shown that when the statistic surface characteristics and targets are found, it is possible to create the filters "whitening" the noise and to construct an optimal detector. In the investigation [7], to minimize clutter created by a random surface, an iterative correlation procedure is used. To detect objects, the "memory effect" is used for the angular correlation function in [8, 9]. In [10], a correlation processing method in the near-field zone with transition from the time to space information concerning the scattered fields is suggested. Further development of this method of phase space with application of the averaged Wigner distribution function was suggested in [11].

However, it should be noted that most of the above-mentioned methods require the preliminary information storage before processing. In this paper, a new method for fast detection of metal objects

Received 4 July 2016, Accepted 29 September 2016, Scheduled 13 October 2016

* Corresponding author: Vladimir Ilich Koshelev (koshelev@lhfe.hcei.tsc.ru).

The authors are with the Institute of High Current Electronics, SB RAS, 2/3 Akademichesky ave., Tomsk 634055, Russia.

near a RRS of medium is studied using ultrawideband (UWB) pulses with orthogonal polarization. A possibility to radiate and record ultrawideband pulses with orthogonal polarization was shown previously in [12, 13] as well as a possibility to construct multielement antenna arrays. Below we will show that in a number of cases this enables recording only maxima of reflected signals and herewith detecting an object located close to RRS.

To simulate the electromagnetic wave scattering from RRS, two classes of numerical methods are used most often [14]. For the problems of scattering by slightly rough surfaces, the integral equation method is preferable. For the problems with rough media and complex geometry, including objects or scatterers, the finite-difference time-domain (FDTD) method is more applicable. The integral equation methods are used for investigations both in frequency and time domain for ultrawideband signals. Method of moments (MM) is used, as a rule, for solution of integral equations by transforming them into the system of linear equations [15–18]. The main problem in the given models is the absence of natural representation for a half-space Green function into the presence of a random rough reflecting surface. Random characteristics of a reflecting surface are usually accounted by means of Monte Karlo method. In [3], several methods are compared. They are the following: method of moments, multilevel fast multipole method, and physical-optical method. Moreover, there are experimental data obtained by the method of aperture synthesizing. In [19, 20], a "four-path" method has been developed by the author. Various approximate models for estimation of field scattering from RRS in the presence of the objects based on the modifications of the integral equation method are presented as well in [21–24].

The FDTD method is comparatively simple. However, exact simulation requires significant computation resources. One of the first complete models of GPR was constructed using FDTD method, though in one-frequency case [25]. The accuracy of the calculation domain simulation for the subsequent more reliable comparison with the experiment was emphasized in the research [26]. To calculate by FDTD method, the real antennas, mine models, ground roughness, water puddles and grass on the surface (using fractal methods) were simulated. When simulating radar for the road surface diagnostics, the symplectic Euler method is used to solve Maxwell equation in time domain [27]. In [5, 6], the computation of the scattered fields was made by FDTD method. In our work, we also use the FDTD method as the most universal.

2. SOFTWARE PROGRAM

To investigate reflection of UWB electromagnetic pulses from the surfaces of a definite shape having the prescribed electric characteristics and containing metal objects, a program based on the finite-difference time-domain method for Maxwell equations [28] has been developed. Basic geometry of the problem presents a three-dimensional parallelepiped with the 3D cell dimensions of $240 \times 240 \times 240$ partially filled with the medium of conductivity σ and relative dielectric permittivity ε. Note that the geometry of the domain of computation in the next Figures is presented without conservation of proportions. A cross-section of the region x-z is presented in Fig. 1. The cross-section of the region y-z is of the same form. To simulate a plane wave falling from free space normally to the surface, an approach consisting in division of the regions of the total and scattered fields (TF/SF) was used. The boundary of these regions is a parallelepiped surface (4 in Fig. 1).

According to this approach, the value of the incident field should be known at any moment of time at the full surface. The difference of this problem from the standard ones, in which a domain decomposition method is used, is that the surface crosses the physical interface of media. So, to assign the incident field inside the medium, a numerical solution of one-dimensional Maxwell equation is used. This approach better matches the calculated fields inside the total field region and outside it (scheme errors and numerical dispersion coincide).

In the program, a completely centered finite-difference Yee scheme is used. Objects and medium are assigned by means of a three-dimensional cell array. Each cell stores one bite of information concerning medium (air, dielectric, metal surface, inside part of metal) for all three electric field components. The characteristics are determined separately for each component due to the shifted grid. The shape of the medium surface is read off from the previously prepared file.

The best choice to match the equations at the open boundaries of the computing area is a completely absorbing layer. For the problem under study, the insertion of the absorbing layer at all the boundaries

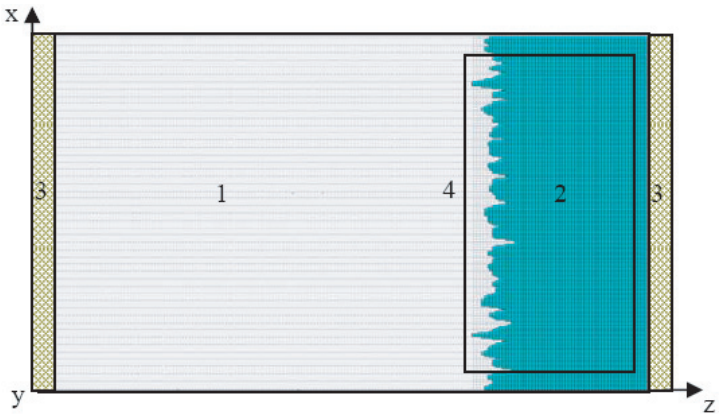

Figure 1. Geometric pattern of the problem: 1 — free space, 2 — dielectric medium , 3 — matched absorbing layer, 4 — boundary surface of the total and scattered field regions.

results in great overhead since the boundaries are located in different media. So, realization of this method results in the insertion of four subsidiary vector quantities in addition to the main fields $\vec{E}$ and $\vec{H}$. When saving the memory, the structure of the internal cycles in the program becomes complicated, and unified equations result in greater memory expenses and large volume of idle computations. Thus, we have chosen a compromise approach: the matched layer method of UPML-type is used at the uniform boundaries by x while at other boundaries the Mur 2nd-order absorbing boundary conditions are applicable. The tests have shown satisfactory use of this approach.

Time and space steps with respect to three coordinates for FDTD computation were $\Delta t \approx 16.7$ ps and $\Delta = 1$ cm, respectively. The program was realized in C++ language for a personal computer with Intel i7 processor; the calculation time of one realization was about 0.5 hour using 1 Gb of RAM.

3. SIMULATION OF A RANDOM ROUGH REFLECTED SURFACE

To obtain a random surface with assigned smoothness, we transmit the normal random stationary uncorrelated process through the filter with the assigned impulse response $h(x, y) = \exp[-(x^2 + y^2)/b^2]$ (Fig. 2). Fig. 3 demonstrates the normal random stationary uncorrelated process $g(x, y)$. Fig. 4 presents a two-dimensional signal $q(x, y)$ at the filter circuit output at $b = 4$ (RRS realization).

Analysis of the results obtained indicates that this approach is applicable for simulation of the surface with the assigned correlation length varying the scale coefficient b.

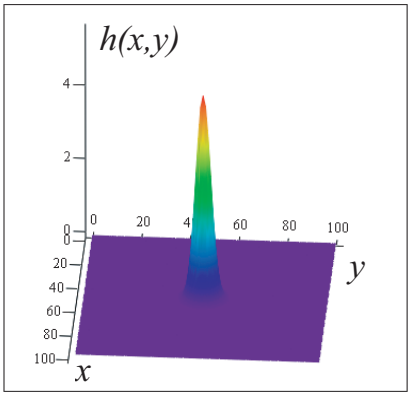

Figure 2. Filter impulse response at $b = 4$.

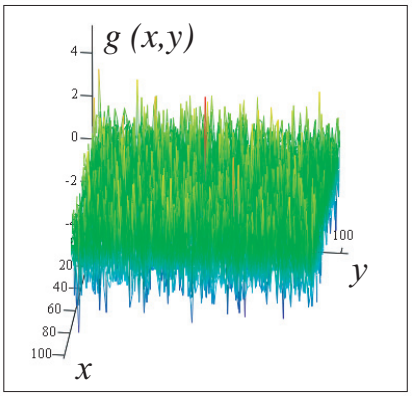

Figure 3. Filter input signal.

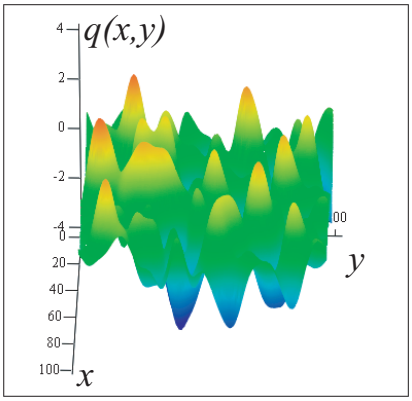

Figure 4. Filter output signal at $b = 4$ (RRS realization).

4. OBJECT DETECTION NEAR A RANDOM ROUGH SURFACE

Here, we consider the problem of the metal object detection against the background of an underlying surface. To solve this problem, we use the following approximations: the underlying surface relief is random and weakly correlated. The effective radar cross section (RCS) of a metal object exceeds RCS of any part of the reflecting surface which in terms of area is comparable with the metal object one. The sounding UWB signal presents two identical three-lobe pulses with linear polarization and plane front edge. The pulses are displaced relative each other in time by the value t_0 equal to the pulse length $\tau_p \approx 0.7$ ns and rotated by 90° (Fig. 5). The central frequency of the sounding pulse spectrum and corresponding wave length were $f_0 = 2$ GHz and $\lambda_0 = 15$ cm, respectively. The receiving process is realized by the antennas oriented by the same polarizations. The effects related to the influence of one polarization to another will be neglected.

To investigate the detection of the metal objects located at the dielectric medium with RRS, the calculations were carried out both with application of the metal object and without it. Further, mutual correlation function $K(\tau) = \langle E^{(1)}(t)E^{(2)}(t - t_0 + \tau)\rangle$ of the received signals with orthogonal polarizations at each receiving point was calculated for each case. Maximum of this function is evidently achieved at the point $\tau = t_0$ corresponding to the relative displacement of the orthogonally polarized pulses at the receiving point. In addition, in view of random roughness of the relief surface, the maximum correlation function value at the point $\tau = t_0$ in the presence of an object can exceed the analogous value without the metal object that will be the criteria of the object detection. To increase the statistical significance of the simulation result, the computations were carried out for 10 different RRS realizations with the subsequent averaging.

Figure 6 presents the simulation scheme where $\tau_p c$ is the sounding pulse spatial length (c is the velocity of light). A metal object 1 was placed to the RRS dielectric medium 2. The reflected signal accumulated at 25 receiving points 3 presenting a 5×5 array located opposite the metal object at a distance $6.5\tau_p c$ from its center. The distance between the receivers was $0.5\tau_p c$.

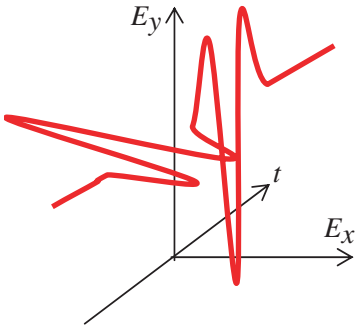

Figure 5. Sounding pulse.

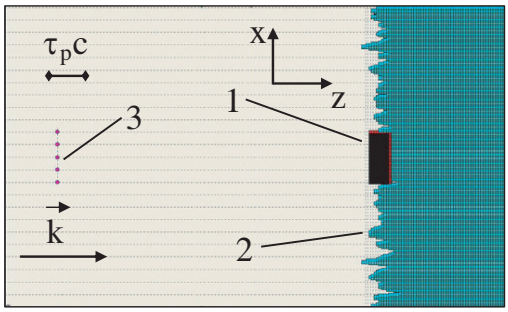

Figure 6. Simulation scheme: 1 — metal object, 2 — dielectric medium with a random rough surface, 3 — receiving array.

For this investigation, we used the RRS relief characterized by the value of the root mean square deviation (RMSD) of the surface from the average level $\sigma_s = 0.14\tau_p c$ and average length of the roughness correlation $l_k = 0.55\tau_p c$. The metal body was a parallelepiped of the thickness $0.5\tau_p c$ and width equal to a half-length. Five different lengths of the space length object $L = (0.8; 1.1; 1.5; 2.2$ and $3)\tau_p c$ were chosen for study. The long side of the object was located along the axis x. When choosing the dimensions of the object L and correlation length l_k, we assumed that the case of the ratios of these close to 1 parameters to λ_0 will be optimum to illustrate the method of metal object detection near a random rough surface. In total, these ratios were the following: $l_k/\lambda_0 \approx 0.73$; $L/\lambda_0 = (1.07; 1.47; 2; 2.9; 4)$. In this case, the ratio l_k/L changes in the limits from 0.69 to 0.18. In future investigations, we suppose to perform the analysis of influence of the correlation length l_k of the rough surface on the possibility of object detection. The objective of the work is representation of the method of metal object detection near a random rough surface.

The dry sandy ground ($\varepsilon = 4$, $\sigma = 0.002\,\mathrm{Sm/m}$) and the sandy ground of the humidity about 12% ($\varepsilon = 10$, $\sigma = 0.07\,\mathrm{Sm/m}$) were chosen as the dielectric medium parameters [29]. These parameters correspond to the medium characteristics at the central frequency of a sounding pulse. Subsequent calculations are carried out in the assumption that frequency dispersion of the electric parameters of the ground is of weak influence [30].

Figure 7 demonstrates the signals reflected from the underlying surface at two perpendicular polarizations in the presence (a) and absence (b) of the metal object.

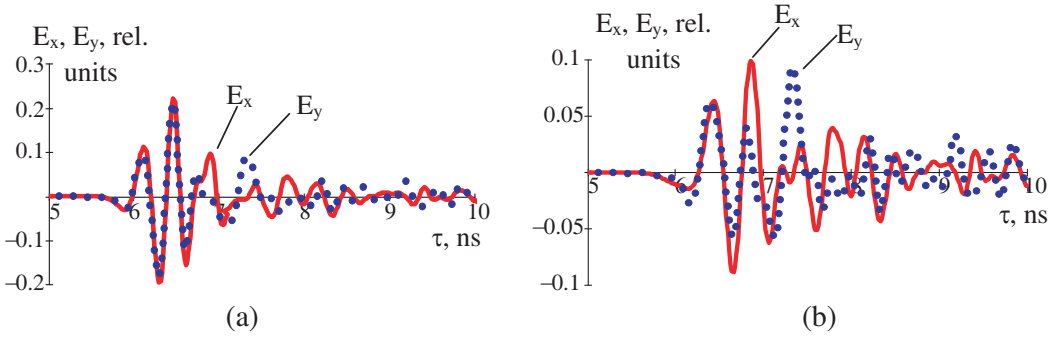

Figure 7. Reflected pulses with orthogonal polarizations: (a) in the presence and (b) in the absence of the object.

Figure 8 presents the result of calculation of the mutual correlation between the orthogonally polarized signals received at one of the points. The diagram shows that correlation at the maximum point $\tau = t_0$ in the presence of the metal object (solid line) exceeds the correlation without the one (dashed line).

Figure 9 presents the values of the correlation functions at $\tau = t_0$ in case of presence (solid line) and absence (dashed line) of the metal object calculated at 25 receiving points.

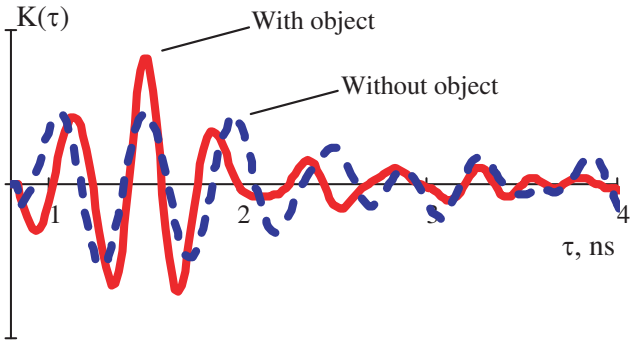

Figure 8. Mutual correlation between the orthogonally polarized reflected signals.

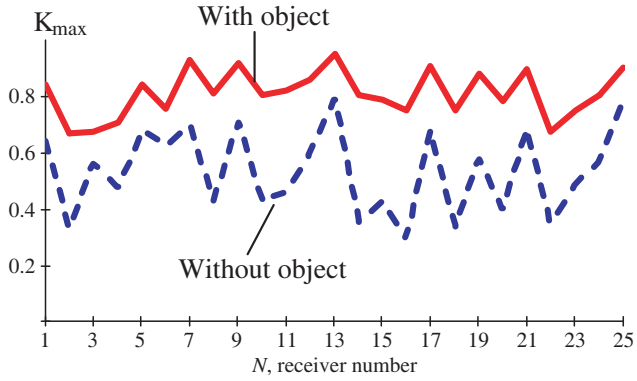

Figure 9. Distribution of the correlation function maxima of the orthogonally polarized reflected pulses.

Figure 10 demonstrates the maximum value of the mutual correlation function $K_{\max}$ of the orthogonally polarized reflected pulses versus the relative dimension of the metal object for the dry (symbols •) and wet (symbols □) ground for one receiving point (central in the receiving array). These symbols for the dry and wet ground will be used in all subsequent diagrams. The value in the diagrams $L/\tau_p c$ equal to zero here and further denotes the absence of the metal object. The interval of RMSD σ_K^0 of the maximum correlation function value in the absence of the body is highlighted in grey. Assume that the body is detected if the interval of RMSD σ_K of the maximum correlation function value in the presence of the object has no interconnection with the σ_K^0 interval. Fig. 10 shows that for one receiving

element, the metal object is detected by the specified criterion at its linear dimensions $L/\tau_p c > 1$ for the dry ground and $L/\tau_p c > 1.5$ for the wet one. In the diagram presented, the RMSD interval corresponds to RRS realizations.

Figure 11 presents the maximum value of the mutual correlation function $K_{\max}$ of the reflected signals versus the metal object dimensions for the dry and wet ground of RRS for the receiving point located at the angle of a 5×5 plane receiving array. One can see from Fig. 11 that the metal object is detected at its linear dimensions $L/\tau_p c > 1$ for the dry ground and only at $L/\tau_p c > 3$ for the wet one.

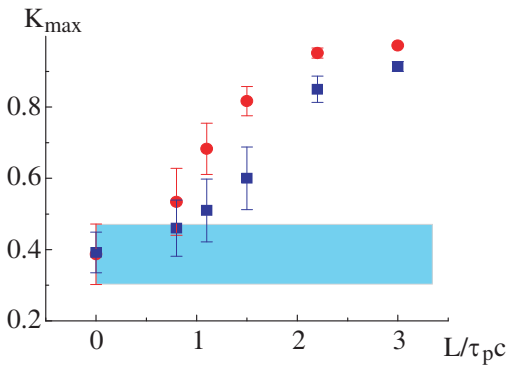

Figure 10. Maximum of the mutual correlation function of the orthogonally polarized reflected signals versus the metal object dimension for the central element of the receiving array for the dry and wet ground: • — dry ground, □ — wet ground.

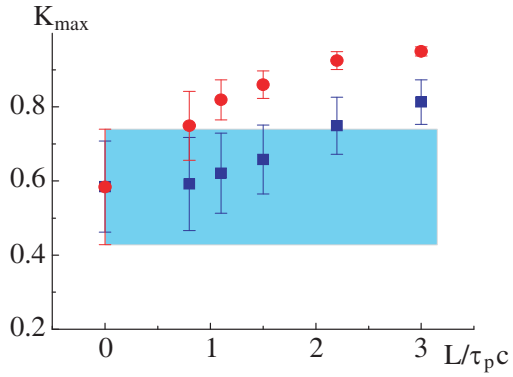

Figure 11. Maximum of the mutual correlation function of the orthogonally polarized reflected signals versus the metal object dimension for the angular element of the receiving array for the dry and wet ground.

Analyzing the data of the diagrams presented in Figs. 10 and 11 as well as the results obtained for other receiving points, a conclusion can be made concerning the possibility to detect metal objects at RRS using a single antenna. However, to decrease the spread of the data at high values of the dielectric permittivity and medium conductivity, it is necessary to increase the number of the elements in the receiving array. In addition, application of multielement arrays allows narrowing the pattern and increasing the signal amplitude.

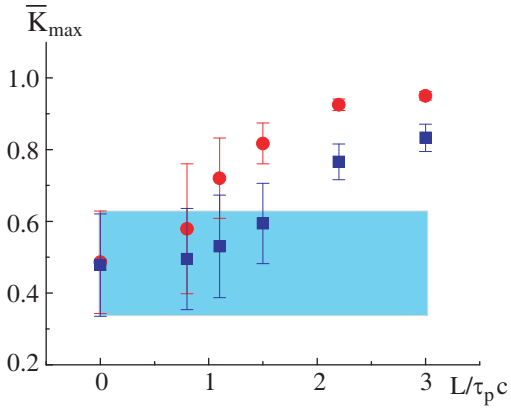

Figure 12. Average maximum values of the mutual correlation function of the orthogonally polarized reflected signals versus the metal object dimension for the linear 5-element receiving antenna for the dry and wet ground.

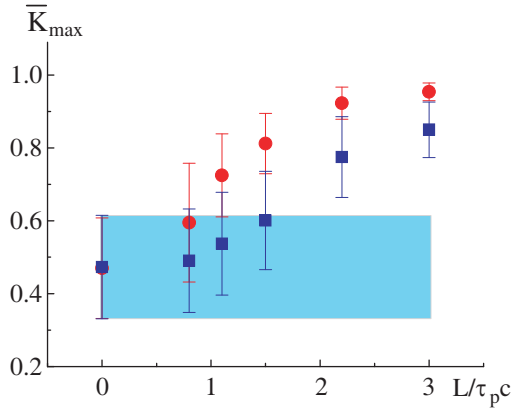

Figure 13. Average maximum values of the mutual correlation function of the orthogonally polarized reflected signals versus the metal object dimension for the plane 25-element receiving array for the dry and wet ground.

Figure 12 shows the average maximum values of the mutual correlation function $\bar{K}_{\max}$ of the orthogonally polarized reflected signals versus the relative dimension of the metal object for the linear 5-element receiving antenna placed perpendicular to the metal object for the dry and wet media. Fig. 13 presents the average maximum values of the mutual correlation function of reflected signals versus the relative dimension of the metal object for a plane (5×5) receiving array consisting of 25 elements. In these calculations, the averaging was carried out both by RRS realizations and by the maximum values of the mutual correlation function of the reflected signals for all elements of the receiving array taken into account. RMSD intervals correspond to the averaging by maximum of the correlation function. We can see from the figures that in case of the dry ground, the object detection by the previously inserted criterion is possible for both cases at $L/\tau_p c > 1$. At the ground humidity of about 12%, the detection is possible only at $L/\tau_p c > 2$.

In case of using a plane 25-element receiving antenna, the additional signal processing is possible allowing increasing the possibility of detection due to the calculation of the mutual correlation between distributions of the reflected signal maxima at the orthogonal polarizations. Fig. 14(a) presents the distribution of the signal maxima for two polarizations at 25 different points of receiving in the presence of the metal object. Fig. 14(b) demonstrates the analogous results in the absence of the object.

The figures show the strong correlation between the distributions of the signal maxima with different polarizations in case the object is present. In case the object is absent, this correlation is absent as well.

Figure 15 demonstrates the values of the correlation coefficients $R = \sum (E^x_{\max} - \bar{E}^x_{\max})(E^y_{\max} - \bar{E}^y_{\max}) / \sigma_{E^x} \sigma_{E^y}$ between the set of the maximum signals with orthogonal polarizations received by different array elements versus relative dimensions of the metal object for the dry (Fig. 15(a)) and wet (Fig. 15(b))

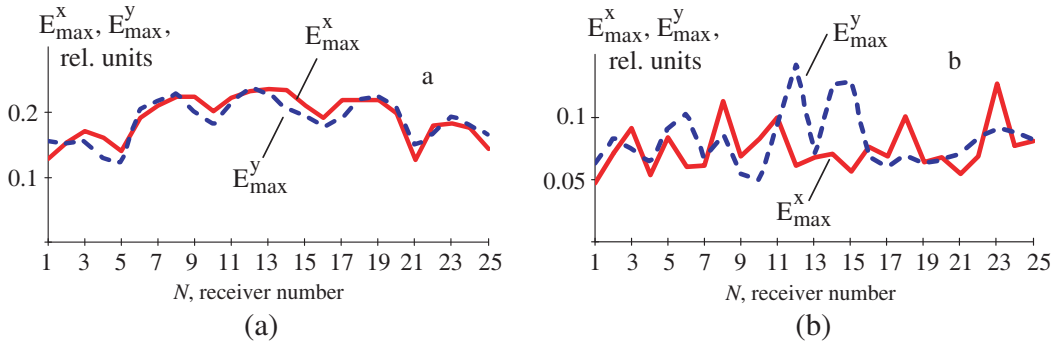

Figure 14. Distribution of the received signal maxima: (a) in the presence of the object; (b) in the absence of the object.

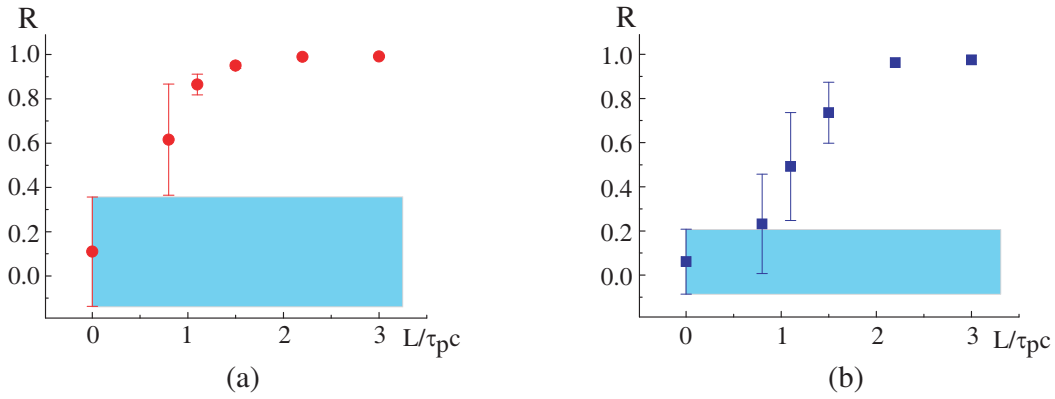

Figure 15. Correlation coefficient of the signal maxima of the orthogonally polarized reflected pulses versus the metal object dimension in case of the (a) dry and (b) wet ground for a 25-element receiving array.

ground. In the calculation data, the averaging was carried out by RRS realizations. One can see from Fig. 15 that the object detection by this method is possible when its linear dimensions are close to the space length of a single sounding pulse. In case the ground is wet, the possibility of detection decreases. However, at $L/\tau_p c > 2$ the difference in the values of the correlation coefficient is absent practically.

5. OBJECT DETECTION UNDER A RANDOM ROUGH SURFACE

An object was placed into the dielectric medium to 4 different depths: Fig. 16(a) — the medial line of the object coincides with the medial line of the surface (coincides with the study in item 4), Figs. 16(b), (c), and (d) — the object is buried to $0.25\tau_p c$, $0.5\tau_p c$ and $0.75\tau_p c$ from position (a), correspondingly. Hereafter, we denote these types of the object location as (a), (b), (c), and (d). To increase the statistical

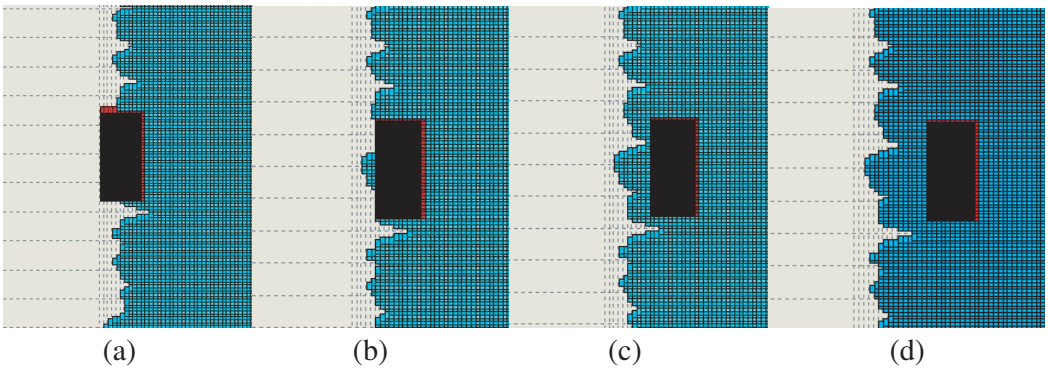

Figure 16. Variants of the metal object location in the dielectric layer under RRS.

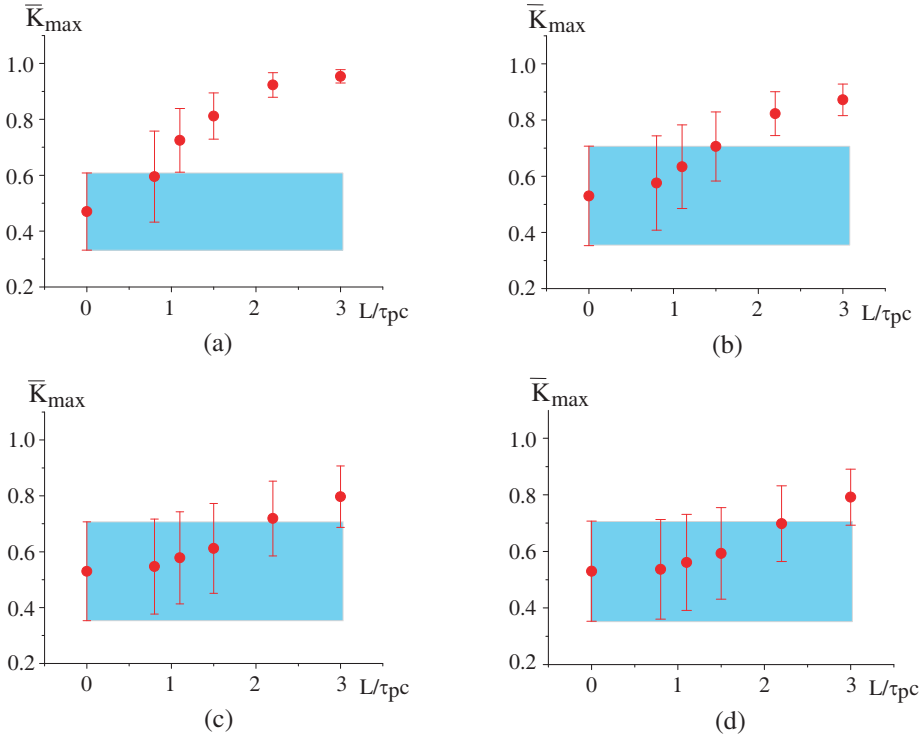

Figure 17. Average maximum values of the mutual correlation function of the orthogonally polarized reflected signals versus the metal object dimension for the dry ground. Figures (a), (b), (c), and (d) correspond to the positions of the object (a), (b), (c), and (d) in Fig. 16.

value of the simulation result, the calculations were carried out for 10 different RRS realizations with the following averaging. A plane 25-element receiving array was used.

Figures 17(a), (b), (c), and (d) present the average maximum values of the mutual correlation function of the reflected signals with orthogonal polarizations versus the metal object dimension for corresponding positions of the metal object (a), (b), (c), and (d) in Fig. 16 for the dry ground.

In these calculations, the averaging was made both by RRS realizations and by the maximum values of the mutual correlation function of the orthogonally polarized reflected signals for all elements of the receiving array taken into account. RMSD intervals correspond to the averaging by the correlation function maxima.

Using a previously introduced criterion, a conclusion can be made that when an object is buried into the dielectric surface, the detection possibility decreases and becomes possible only at the object dimensions $L/\tau_p c > 2$ for position (b) and $L/\tau_p c \geq 3$ for positions (c) and (d).

Figures 18(a), (b), (c) and (d) present the values of the correlation coefficients R between the set of the maximum signals with the orthogonal polarizations received by different array elements versus the metal object dimension for the corresponding positions of the metal object (a), (b), (c), and (d) in Fig. 16 for the dry ground. In the calculations, the averaging was made by RRS polarizations.

Figure 18 shows that when the object is buried into dielectric medium, the possibility of detection by this method decreases and at the position (d) the object is detected only at $L/\tau_p c > 3$.

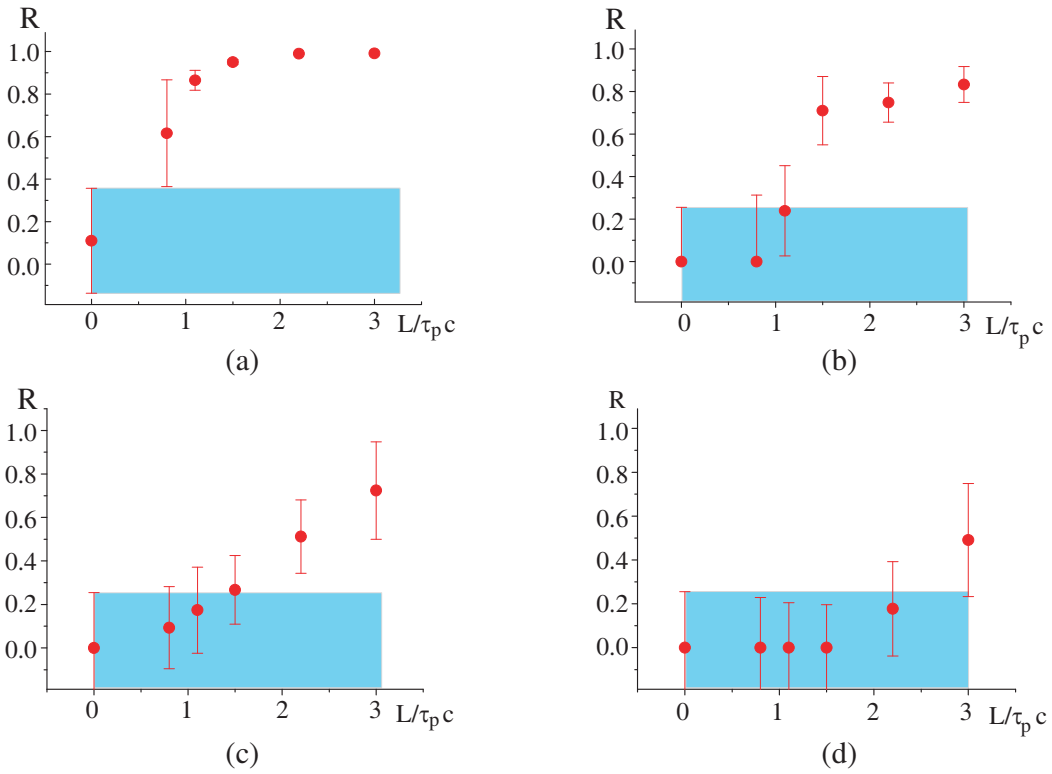

Figure 18. Correlation coefficient of the signal maxima of the orthogonally polarized reflected pulses versus the metal object dimension in case of the dry ground. Figures (a), (b), (c), and (d) correspond to the object positions (a), (b), (c), and (d) in Fig. 16.

Figures 19(a), (b) demonstrate the average maximum values of the mutual correlation function of the orthogonally polarized reflected signals versus the metal object positions (a) and (b) (Fig. 16) for the wet ground. The diagram allows making a conclusion that for the object location in the position (a), the detection is possible at the object dimensions $L/\tau_p c > 2$. When the object is buried into the dielectric surface, the detection possibility is decreased and practically absent for the body positions (c) and (d) (the diagrams for these positions are not presented).

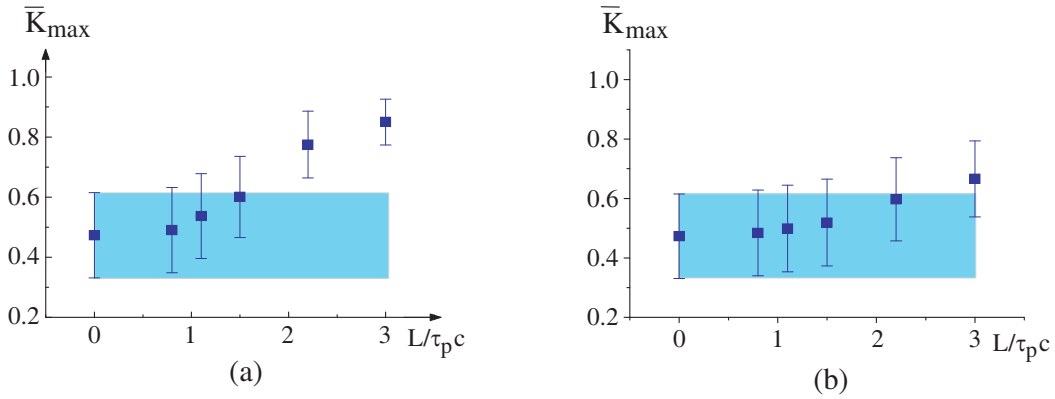

Figure 19. Average maximum values of the mutual correlation function of the orthogonally polarized reflected signals versus the metal object dimension for the wet ground. Figures (a) and (b) correspond to the object positions (a) and (b) in Fig. 16.

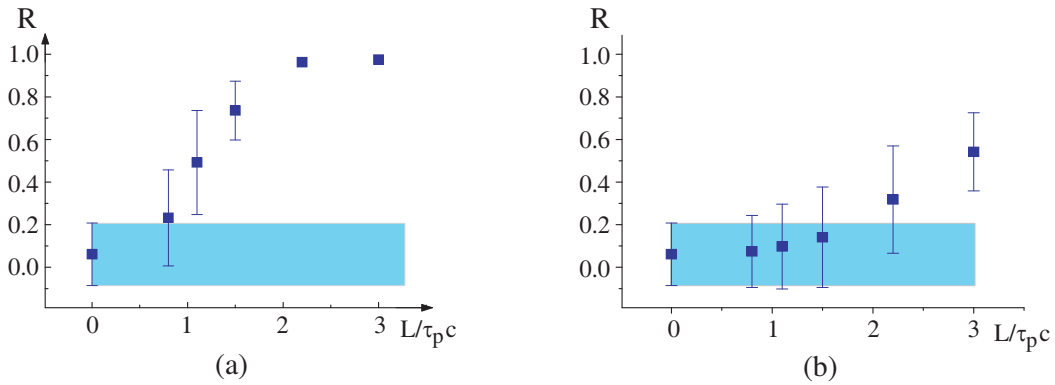

Figure 20. Correlation coefficient of the signal maxima of the orthogonally polarized reflected pulses versus the metal object dimension in case of the wet ground. Figures (a) and (b) correspond to the object positions (a) and (b) in Fig. 16.

Figures 20(a) and (b) show the values of the correlation coefficients R between the set of the maximum signals with orthogonal polarizations received by different array elements versus the metal object dimension for the corresponding positions of the metal object (a) and (b) in Fig. 16 in case of the wet ground.

Figure 20 demonstrates that the object detection by this method is possible when its linear dimensions are close to the space length of a single sounding pulse for the object position (a). At further penetration of the object into the dielectric medium, the detection possibility by means of this method decreases and is practically absent for the body positions (c) and (d) (the diagrams for these positions are not presented).

6. OBJECT DETECTION ABOVE A RANDOM ROUGH SURFACE

Possibility to detect the cross-shaped metal objects located above the surface with RRS was investigated.

A metal body presented 2 crossed parallelepipeds of the thickness $0.2\tau_p c$ and arm width $0.3\tau_p c$ (Fig. 21). Seven different lengths of the object arm were chosen for the study: from $L = \tau_p c$ to $L = 4\tau_p c$ with the arm step of $0.5\tau_p c$. The object was located above the dielectric medium at a distance $0.75\tau_p c$ from the average surface level. In addition, the metal object was turned in the plane x-y through 30° with respect to the coordinate axis and, correspondingly, with respect to the direction of the electric-field vector.

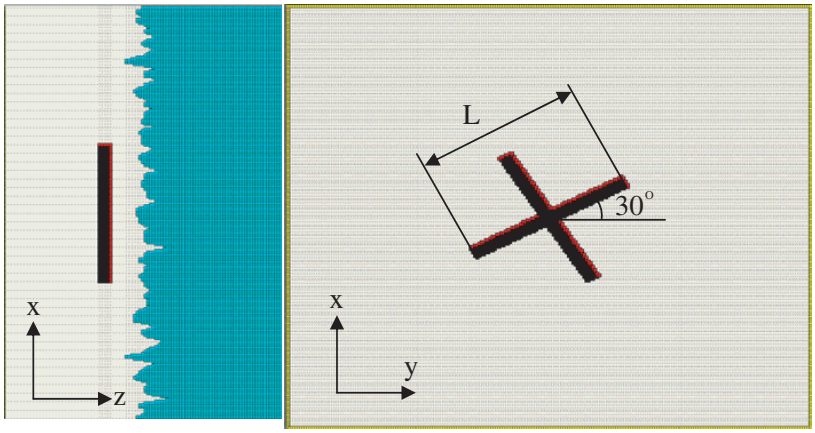

Figure 21. Configuration of the metal object above RRS: (a) x-z cross-section, (b) x-y cross-section.

Figure 22 presents the average maximum values of the mutual correlation function $\bar{K}_{\max}$ of the orthogonally polarized reflected signals versus the metal object dimension $L/\tau_p c$ for the dry (Fig. 22(a)) and wet (Fig. 22(b)) ground.

In the calculations, the averaging was made both by the RRS realizations and by the maximum values of the mutual correlation function of the orthogonally polarized reflected signals for all elements of a plane receiving array taken into account. RMSD intervals correspond to the averaging by the correlation function maxima.

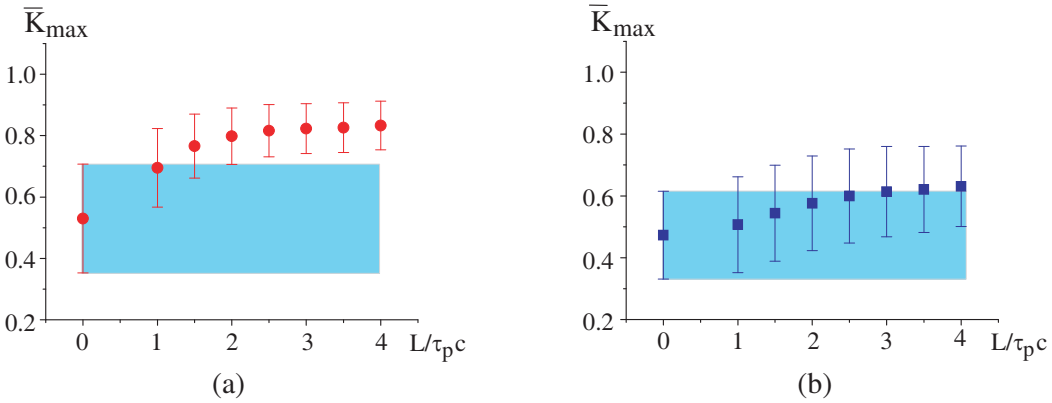

Figure 22. Average maximum values of the mutual correlation function of the orthogonally polarized reflected signals versus the metal object dimension in case of the (a) dry and (b) wet ground for a 25-element receiving array.

By means of the previously introduced criterion, a conclusion can be made that in case of the dry ground the detection is possible at the object dimensions $L/\tau_p c > 2$. As soon as the ground moisture increases, the possibility of detection by this method becomes complicated.

Figure 23 presents the values of the correlation coefficients R between the set of the maximum signals with orthogonal polarizations received by different elements of a plane array versus the metal object dimension in case of the dry (Fig. 23(a)) and wet (23(b)) medium. In the calculations, the averaging was made by RRS realizations.

Figure 23(a) demonstrates that detection of the object located above the dry surface is possible at its dimensions $L/\tau_p c > 1$. In case of the wet ground of RRS, the object is detected reliably at its dimensions $L/\tau_p c \geq 2$ (Fig. 23(b)).

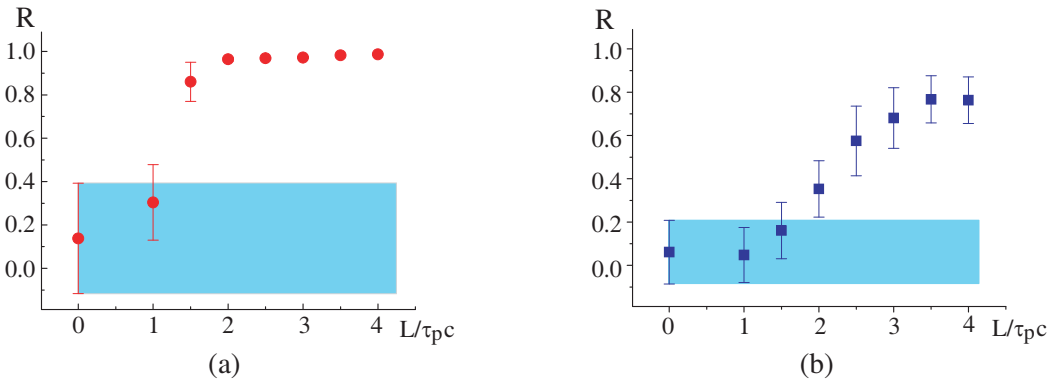

Figure 23. Correlation coefficient of the signal maxima of the orthogonally polarized reflected pulses versus the metal object dimension in case of the (a) dry and (b) wet ground for a 25-element receiving array.

7. CONCLUSION

The method of the metal object detection against the RRS ground by the consecutive nondelay UWB pulses with orthogonal polarizations has been suggested and tested.

Calculations have shown that possibility to detect a metal object against the RRS background depends both on the dimensions of the object itself relative to the chosen space length of a sounding pulse and correlation length of the rough surface and on the ground parameters. Increase of the dielectric permittivity and ground conductivity results in the decrease of the object detection possibility. Application of the mutual correlation function of the orthogonally polarized reflected signals allowed realizing the detection of large objects at a small number of the receiving array elements. Multielement receiving array increases the possibility to detect small-dimensional objects at the calculation of the correlation coefficient between the distributions of the reflected signal maxima.

The developed method allows detecting objects under RRS if their linear dimension is twice longer than the space length of the pulse in case of the dry ground and the depth of the object location equals to 0.2 of the pulse space length. Increase of the object burial depth and medium humidity results in sharp decrease of the object detection possibility when using UWB pulses with the central frequency of the radiation spectrum equal to 2 GHz.

Detection of a cross-shaped object located over RRS by this method is possible in case its dimensions exceed the pulse space length.

ACKNOWLEDGMENT

The authors are thankful to S. E. Shipilov and V. T. Sarychev for helpful discussions.

REFERENCES

1. Daniels, D. J., *Ground Penetrating Radar*, 2nd edition, The Institution of Electrical Engineers, London, 2004.
2. Carin, L., N. Geng, M. McClure, J. Sichina, and L. Nguyen, "Ultrawide-band synthetic-aperture radar for mine-field detection," *IEEE Antennas and Propagation Magazine*, Vol. 41, No. 2, 18–33, 1999.
3. Sullivan, A., R. Damarla, N. Geng, Y. Dong, and L. Carin, "Ultrawide-band synthetic aperture radar for detection of unexploded ordnance: Modeling and measurements," *IEEE Transactions on Antennas and Propagation*, Vol. 48, No. 9, 1306–1315, 2000.
4. Taylor, J. D., *Ultra Wideband Radar Technology*, CRC Press, 2001.

5. Dogaru, T. and L. Carin, "Time-domain sensing of targets buried under a rough air-ground interface," *IEEE Transactions on Antennas and Propagation*, Vol. 46, No. 3, 360–372, 1998.
6. Dogaru, T., L. Collins, and L. Carin, "Optimal time-domain detection of a deterministic target buried under a randomly rough interface," *IEEE Transactions on Antennas and Propagation*, Vol. 49, No. 3, 313–326, 2001.
7. Rappaport, C., M. El-Shenawee, and H. Zhan, "Suppressing GPR clutter from randomly rough ground surfaces to enhance nonmetallic mine detection," *Subsurface Sensing Technologies and Applications*, Vol. 4, No. 4, 311–326, 2003.
8. Zhang, G. F. and L. Tsang, "Angular correlation function of wave scattering by a random rough surface and discrete scatterers and its application in the detection of a buried object," *Waves in Random Media*, Vol. 7, 467–478, 1997.
9. Zhang, G. F., L. Tsang, and Y. Kuga, "Studies of the angular correlation function of scattering by random rough surfaces with and without a buried object," *IEEE Transactions on Geoscience and Remote Sensing*, Vol. 35, No. 2, 444–453, 1997.
10. Cmielewski, O., M. Saillard, and H. Tortel, "Detection of buried objects beneath a rough surface," *Waves in Random and Complex Media*, Vol. 16, 417–431, 2006.
11. Morelle, N., M. Testorf, N. Thirion-Moreau, and M. Saillard, "Electromagnetic probing for target detection: Rejection of surface clutter based on the Wigner distribution," *Journal of the Optical Society of America A-optics Image Science and Vision*, Vol. 26, No. 5, 1178–1186, 2009.
12. Efremov, A. M., V. I. Koshelev, B. M. Kovalchuk, V. V. Plisko, and K. N. Sukhushin. "Generation and radiation of high-power ultrawideband nanosecond pulses," *Journal of Communications Technology and Electronics*, Vol. 52, No. 7, 756–764, 2007.
13. Balzovskii, E. V., Y. I. Buyanov, and V. I. Koshelev, "Dual polarization receiving antenna array for recording of ultra-wideband pulses," *Journal of Communications Technology and Electronics*, Vol. 55, No. 2, 172–180, 2010.
14. Warnick, K. F. and W. C. Chew, "Numerical simulations methods for rough surface scattering — Topical Review," *Waves in Random Media*, Vol. 11, R1–R30, 2001.
15. O'Neill, K., R. F. Lussky, Jr., and K. D. Paulsen, "Scattering from a metallic object embedded near the randomly rough surface of a lossy dielectric," *IEEE Transactions on Geoscience and Remote Sensing*, Vol. 34, No. 2, 367–376, 1996.
16. Geng, N. and L. Carin, "Wide band electromagnetic scattering from a dielectric BOR buried in a layered lossy dispersive medium," *IEEE Transactions on Antennas and Propagation*, Vol. 47, No. 4, 610–619, 1999.
17. Wang, X., C. F. Wang, Y. B. Gan, and L. W. Li, "Electromagnetic scattering from a circular target above or below rough surface," *Progress In Electromagnetics Research*, Vol. 40, 207–227, 2003.
18. Guan, B., J. F. Zhang, X. Y. Zhou, and T. J. Cui, "Electromagnetic scattering from objects above a rough surface using the method of moments with half-space Green's function," *IEEE Transactions on Geoscience and Remote Sensing*, Vol. 47, No. 10, 3399–3405, 2009.
19. Johnson, J. T., "Numerical study of scattering from an object above a rough surface," *IEEE Transactions on Antennas and Propagation*, Vol. 50, No. 10, 1361–1367, 2002.
20. Johnson, J. T. and R. J. Burkholder, "A study of scattering from an object below a rough surface," *IEEE Transactions on Geoscience and Remote Sensing*, Vol. 42, No. 1, 59–66, 2004.
21. Ji, W.-J. and C.-M. Tong, "The E-PILE+SMCG for scattering from an object below 2D soil rough surface," *Progress In Electromagnetics Research B*, Vol. 33, 317–337, 2011.
22. Bakr, S. A. and T. Mannseth, "An approximate hybrid method for electromagnetic scattering from an underground target," *IEEE Transactions on Geoscience and Remote Sensing*, Vol. 51, No. 1, 99–107, 2013.
23. Afifi, S., B. Mokhtar, R. Dusseaux, and A. Berrouk, "Electromagnetic wave scattering from rough layered interfaces: Analysis with the small perturbation method and the small slope approximation," *Progress In Electromagnetics Research B*, Vol. 57, 177–190, 2014.

24. Altuncu, Y., "A numerical method for electromagnetic scattering by 3-D dielectric objects buried under 2-D locally rough surfaces," *IEEE Transactions on Antennas and Propagation*, Vol. 63, No. 8, 3634–3643, 2015.
25. Bourgeois, J. M. and G. S. Smith, "A complete electromagnetic simulation of the separated-aperture sensor for detecting buried land mines," *IEEE Transactions on Antennas and Propagation*, Vol. 46, No. 10, 1419–1426, 1998.
26. Giannakis, I., A. Giannopoulos, and C. Warren, "A realistic FDTD numerical modelling framework of ground penetrating radar for landmine detection," *IEEE Journal of Selected Topics in Applied Earth Observations and Remote Sensing*, Vol. 9, No. 1, 37–51, 2015.
27. Fang, H., G. Lin, and R. Zhang, "The first-order symplectic euler method for simulation of GPR wave propagation in pavement structure," *IEEE Transactions on Geoscience and Remote Sensing*, Vol. 51, No. 1, 93–98, 2013.
28. Taflove, A. and S. C. Hagness, *Computational Electrodynamics: The Finite-Difference Time-Domain Method*, 2nd edition, Artech House, Boston, MA, 2000.
29. Leschanskiy, I., G. N. Lebedeva, and V. D. Schumilin, "Electrical parameters of sandy and loamy soils in the range of centimeter, decimeter and meter wavelength," *Radiophysics and Quantum Electronics*, Vol. 14, No. 4, 445–451, 1971.
30. Teixeira, F. L., W. C. Chew, M. Straka, M. L. Oristaglio, and T. Wang, "Finite-difference time domain simulation of ground penetrating radar on dispersive, inhomogeneous, and conductive soils," *IEEE Transactions on Geoscience and Remote Sensing*, Vol. 36, No. 11, 1928–1937, 1998.